10

Influence of tellurium and zinc stoichiometry on the ellipsometric spectra of ZnTe/GaAs (100)

© A.A. Grekova[1,2], E.A. Klimov[1], A.N. Vinichenko[1,2], I.D. Burlakov[1]

[1] Joint Stock Company „NGO Orion„Orion, Moscow, Russia
[2] National Research Nuclear University „MEPhI", Moscow, Russia

E-mail: ingo.tyan2@mail.ru

Received January 13, 2024
Revised January 27, 2025
Accepted February 28, 2025

The effect of Zn : Te molecular flux stoichiometry on the optical properties of zinc telluride was studied. The considered ZnTe structures were obtained on GaAs (100) substrates using molecular beam epitaxy. The ellipsometric spectra of the ψ parameter were determined using optical ellipsometry. The study showed that the Van Hove singularities E_1 and $E_1 + \Delta_1$, corresponding to 3.65 eV and 4.27 eV, are characteristic of the ZnTe compound. Excess tellurium in the incident substance flux leads to a simultaneous decrease in the amplitude and broadening of the extrema in the psi(lambda) spectrum due to the formation of defects that absorb visible radiation. The spectra of the psi parameter and the imaginary component of the permittivity in the $\psi(\lambda)$ region have extrema that are similar in energy position. When one of the components prevails in the Zn:Te ratio, the energy positions of the critical points remain constant at different sample thicknesses. However, excess Zn in the Zn:Te ratio leads to uncertainty in the energy position of the absorption edge. The results of the study will be useful for ellipsometric express control of stoichiometry and assessment of the crystalline quality of binary solid solutions of the A_2B_6 group in the composition of epitaxial layers

Keywords: zinc telluride, spectral ellipsometry, molecular beam epitaxy, composition stoichiometry, ellipsometric spectra.

DOI: 10.61011/EOS.2025.03.61160.5-25

1. Introduction

Devices employing the physical principles of optoelectronics have been attracting attention because of the ability to convert light energy into electrical energy. Solar cells, thermal imaging devices, and modulators are designed based on them [1–4]. GaN, CdHgTe, and ZnTe are the main materials of the above devices because of the existence of direct-gap electronic transitions in them [5–7].

Structures based on ternary solid solution of CdHgTe (CMT) along with microbolometer systems and InSb structures, are the most commonly used structures in modern IR devices. The initial purity of the materials used and the structural quality of the heterostructures directly affect the performance of the final devices, so molecular beam epitaxy (MBE) and chemical vapor deposition (CVD) methods are mainly used to obtain high crystalline perfection of the structures of group A_2B_6. The CMT ternary solid solution exhibits significant lattice parameter mismatch with most commercially available substrate materials, except for CdZnTe (CZT). Alternative Si, GaAs substrates are used for the industrial synthesis of CMT-based structures because of the challenges of the preparation of epi-ready CMT substrates and their low availability. However, in order to obtain device structures of proper quality on substrates with lattice mismatch $\sim 19\%$ for Si and $\sim 14\%$ for GaAs, it is necessary to first synthesize buffer layers with high structural perfection, one of which is the ZnTe layer (7.6 % mismatch between the lattice parameters of ZnTe and GaAs). Additive or, as they are also called, nucleated ZnTe thin layers are used in the synthesis of CMT-based heterostructures on alternative materials to preserve the crystallographic orientation of the substrate in the overlying [8] layers, as well as for smooth relaxation of mechanical stresses by comparison with CdTe. Moreover, the surface morphology of the growing ZnTe film can be improved by adding atomic zinc to the main stream of zinc telluride binary compound [9].

Two *in situ* methods are employed for monitoring the growth of A_2B_6 group structures: reflection high-energy electron diffraction (RHEED) and optical ellipsometry. Both methods prove useful in obtaining the necessary information about the structural quality of the substrate during surface preparation prior to the growth process and the growing epitaxial film. The ellipsometry method also allows determining the substrate surface temperature during the epitaxial growth process.

The actual task is to determine the impact of the stoichiometry of binary solid solutions A_2B_6 on the optical characteristics of the grown structure using the spectral ellipsometry method. The set task is resolved by using the relationship between the critical points on the ellipsometric spectrum of the parameter ψ and the Van-Hove features observed in the density of electronic states or on the

spectrum of the imaginary dielectric constant. The results of this study will be useful for qualitative determination of the stoichiometric composition of epitaxially grown binary ZnTe compounds, while the analysis of ellipsometric spectra ψ can be an used as an indirect express method for determining the presence of defects in samples affecting the electrophysical and structural properties of ZnTe films.

Samples and research methods

ZnTe films (samples № 21 and № 22) were grown by MBE in an ultrahigh vacuum multi-chamber Riber Epineat Cluster on semi-insulating epi-ready GaAs (100) substrates using a binary ZnTe source and molecular Te and Zn sources. Zn flux was added to the ZnTe flux generated by the binary source for growing sample № 21 and Te_2 flux was added to ZnTe flux for growing sample № 22. Temperature was monitored by using thermocouple embedded in the sample heater and an *in situ*-calibrated pyrometer Ircon Modline 5. The growth of the films was accompanied by *in situ*-monitoring of the crystal quality using the RHEED system. A retractable Bayard-Alpert sensor was used to measure molecular fluxes. Pre-growth preparation of the GaAs substrate was carried out in the classical way in two stages: degassing of the sample holder with the substrate for removal of volatile compounds and water vapor was carried out in the pre-treatment chamber at a temperature of 350 °C for 20 min. After that, the desorption of natural oxides was conducted in arsenic flow at $680\ {}_3$C for 5 min followed by the growth of 0.5 μm thick GaAs buffer layer in the growth reactor of materials of group A_3B_5. Next, the holder with the substrate was moved to the growth chamber of materials of group A_2B_6 to synthesize ZnTe films. ZnTe films were grown at a substrate temperature of 400 °C.

After epitaxial growing of ZnTe films the samples were unloaded from the MBE unit and measured by atomic force microscopy using NT-MTD Ntegra Maximus microscope in semi-contact mode in $5 \times 5\,\mu$m field. The RMS roughness (R_q) of the surface of the grown films were 1.31 nm for sample № 21 and 1.83 nm for sample № 22, respectively. The sample grown with the addition of Zn was found to have better surface morphology than the sample grown with the added tellurium.

The spectra of ellipsometric parameters ψ (amplitude) and Δ (phase) of the studied samples were measured under normal conditions using EGS01A-UIX2 spectral ellipsometer manufactured by Beijing Ellitop Scientific Co.Ltd (China) in the wavelength range of 250−2500 nm (from 0.496 to 4.96 eV) with a step of 2 nm. The angle of incidence of the light beam to the sample plane was 70^{σ}. Deuterium (250−400 nm) and halogen lamps (450−2500 nm) were used as the illumination source.

SEM images of the samples were obtained using a Prisma E SEM Thermo Fisher Scientific (USA) scanning electron microscope.

Results and discussion

The electronic and optical properties are determined by the structural features of the crystal lattice and the electron density found on the surface or in volume of the material. Thus, the information about the crystal structure parameters of the grown film can be obtained by analyzing the optical, infrared or X-ray absorption, reflectance and transmittance spectra or conductivity characteristics. These parameters are characterized by critical symmetry points or Van Hove features [10]. They are often defined precisely in the density of electronic states and in the zone structure of the material as extremes and indicate interzone transitions of electrons in materials. The energy positions of these extrema correspond to the energies of occurrence of intrinsic, optical, exciton, or exciton-phonon absorptions [11].

Also, the structural features and their characterizing critical points of epitaxial films, including ZnTe, can be interpreted by the spectra of the dielectric constant component or refractive and absorption coefficients n and k, respectively. The decomposition of the experimentally obtained dielectric permittivity into real and imaginary components is used to determine the energy position of the critical points [12,13]. The calculation of these functions consists of solving the inverse problem of ellipsometry at each wavelength from the initial approximation. A theoretical ellipsometric model of the parameters ψ and Δ for the ZnTe material was used as such an approximation in this study [14].

The solution of the inverse problem of ellipsometry with known thicknesses of ZnTe films as well as optical parameters n, k of GaAs substrate was used to calculate the dielectric permittivity components [14]:

$$\mathrm{tg}\,\Psi(\lambda)e^{i\Delta(\lambda)} = F(n(\lambda), k(\lambda), d, \varepsilon_1(\lambda), \varepsilon_2(\lambda)), \qquad (1)$$

where n — the refractive index of the individual layer, k — the absorption index of the individual layer, d — the thickness of the individual layer, ε_1 — the real component of the dielectric constant of the individual layer, ε_2 — the imaginary component of the dielectric constant of the individual layer.

The convergence of the experimental (ψ_{exp} and Δ_{exp}) and calculated (ψ_{cal} and Δ_{cal}) spectra is determined by achieving a minimum mismatch of the parameter q at all wavelengths:

$$q = \sum_i \left(\frac{(\Psi_{\mathrm{exp}} - \Psi_{\mathrm{cal}})^2}{(\delta\Psi)^2} + \frac{(\Delta_{\mathrm{exp}} - \Delta_{\mathrm{cal}})^2}{(\delta\Delta)^2} \right), \qquad (2)$$

where $\delta\Psi$, $\delta\Delta$ are normalization multipliers. The adequacy of the model was determined by the minimum achieved function value q. In case of failure to achieve an adequate value, the structure model was complicated and the minimization of the function q was performed again.

The Cauchy model was used to study the values $n(\lambda)$, $k(\lambda)$ of oxide films as weakly absorbing media:

$$n(\lambda) = n_0 + \frac{A}{\lambda^2} + \frac{B}{\lambda^4}, \qquad (3)$$

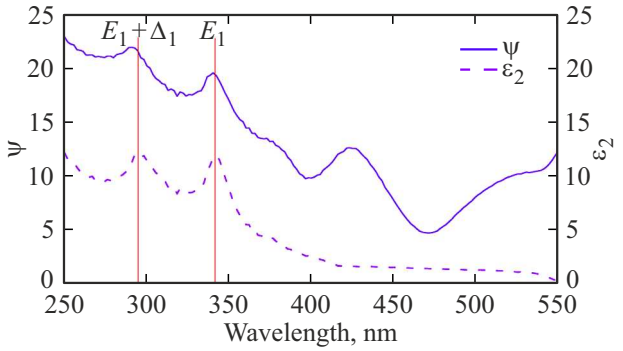

Figure 1. The dependence of the parameters ψ (solid curve), ε_2 (dashed curve) on the wavelength of the incident radiation. The red straight lines and arrows in the plot indicate the wavelengths corresponding to the critical points of the structure.

$$k(\lambda) = \frac{C}{\lambda^2} + \frac{D}{\lambda^4}, \tag{4}$$

where A, B, C, D are unknown constants to be determined.

The Cauchy model represented by equation (2) was used as a model of the oxide layer on the ZnTe surface. The optical parameters obtained with this model matched the literature data: $n = 1.9$, $k = 0.01$ [15].

Fig. 1 shows the calculation result of the imaginary component of the dielectric permittivity (ε_2) and the experimentally obtained spectrum of the ellipsometric parameter ψ in the opaque part for the ZnTe sample with prevalent Zn in the Zn:Te stoichiometry. The greatest interest attracted by this region of the spectrum (from 250 to 550 nm) is explained by the fact that the energy corresponding to this waveband exceeds the energy of the band gap of ZnTe. Therefore, the many extrema encountered in this section correspond to the absorption of radiation, and hence the optical and electronic characteristics of the grown material [11].

The parameter Δ is directly related to the roughness of the sample, due to which the accuracy of determining the critical points is reduced; therefore, it is reasonable to use exactly the spectrum ψ to analyze the composition of epistructures [16,17].

Fig. 2 shows images of the acquired ZnTe structures in the case of prevalent tellurium (a) or zinc (b) in the incident stoichiometry. As shown in Fig. 1, due to the lack of sample rotation during growth, the ZnTe structures possessed a color gradient, which may indicate inhomogeneity in thickness. Therefore, the spectra of ellipsometric parameters were taken with a step of 5 mm, starting from the first region and ending with the third one, indicated in Fig. 2. Fig. 3 also shows dependences of ψ on the wavelength of the incident radiation in the case of the prevalence of tellurium or zinc in the obtained ZnTe solid solution on GaAs (100) substrate. The values of the energies as well as the wavelengths at each critical point are listed in Table 1. The region 1 (Fig. 2) of the grown structures turned out to be the most informative according to the experimental data.

In our case, the exact energy positions of the Van-Hove features were determined using the spectrum ε_2 in the region of $E > E_g$ ($\lambda < 550$ nm) as shown in Fig. 1 and presented in Tables 1 and 2. The comparison with the extrema of the spectrum ψ in the same energy range, according to Table 2, showed that the roughness has the lowest effect on the shifting of the symmetry point E_1 (0.0012 eV or 0.14 nm), and it has the strongest effect on $E_1 + \Delta_1$ (0.07 eV or 5.14 nm). Thus, it is shown that it is sufficient to use the spectrum $\psi(\lambda)$, instead of $\varepsilon(\lambda)$ (Fig. 1), to determine the positions of the Van-Hove critical points for a significant simplification of the computational model.

The critical point E_0 corresponds to the band gap energy and is directly related to the intrinsic absorption of the material. Heating of the sample is the cause of phonon oscillations in the crystal lattice and leads to a shift in the energy position E_0 [17]. The oscillations beyond the absorption edge ($E < E_g$) indicate interference of the incident radiation due to the variation of the absorption index in the material volume. The increase of the absorption index results in a decrease of the amplitude of interference oscillations [18,19]. Usually, the absorption edge in thick samples, corresponds to the onset of interference in $\psi(\lambda)$ starting at about 900 nm [17,18]. The spectrum ψ has interference oscillations also in the opacity region of the film ($E > E_g$) due to the small thickness of ZnTe films № 21 and № 22 films as shown in Fig. 3 and 4. Therefore, it is not possible to define E_g explicitly. Thus, as shown in this study, it is reasonable to identify the absorption edge based on the spectrum ε_2 or absorption index k in the region of linear transmission drop (Fig. 1) [13]. In addition, doubly ionized intrinsic defects formed in the sample volume especially near the surface in the case of excess zinc in the molecular flux of the compounds A_2B_6 [20], may lead to scattering of the incident radiation. In turn, such defects can create additional stress in the crystalline lattice [21]. Thus, the comparison of samples № 21 and № 22 showed that the absorption edge is „blurred“ in the visible radiation region because of the formation of acceptor defects in the material volume (Tables 1 and 2).

The temperature fluctuation during film formation affects the optical absorption at the critical points E_1 and $E_1 + \Delta_1$, but to a negligible extent, so these points are best suited to characterize the composition of the grown structure [19]. The relative shift of critical point positions does not exceed 0.03 % with a substrate temperature control accuracy of $\pm 0.5^\circ$ during epitaxial growth.

The energy positions of the critical points E_1, $E_1 + \Delta_1$, and E_0 indicated in Table 1 are similar to those reported in the literature [12,22] for this material.

As shown in Fig. 3, despite the similar nature of the dependence of the ellipsometric parameter ψ on the wavelength of the incident radiation, the amplitude extrema for samples № 21 and № 22 coincide only for the critical point E_1. In other cases, the prevalence of tellurium in

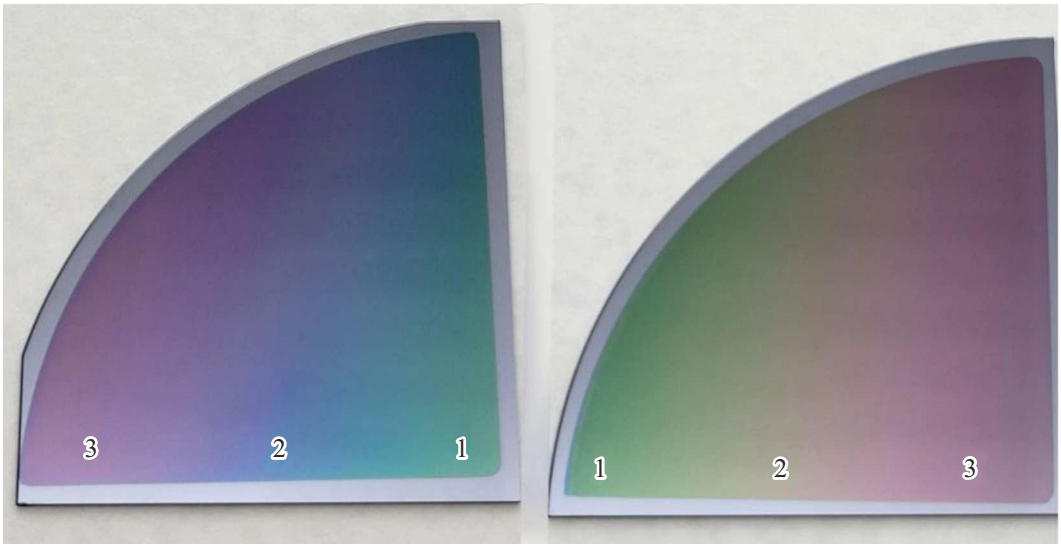

Figure 2. Photographs of ZnTe structures: (*a*) sample № 22, (*b*) sample № 21. Numbers indicate areas in which ellipsometric measurements were made.

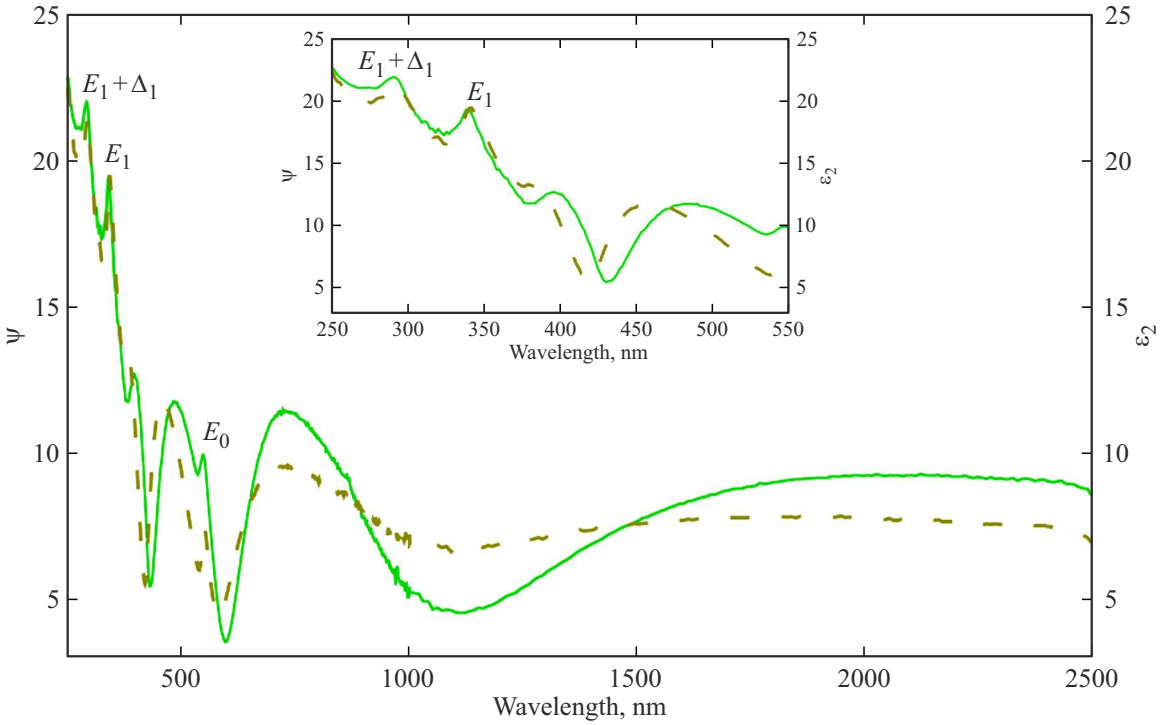

Figure 3. Dependence of the parameter ψ on the wavelength of the incident radiation. The solid curve — sample No 21, the dashed curve — sample No 22. Extremes corresponding to the critical points of the structures are marked.

the incident flux and, consequently, in the ZnTe structure reduces the amplitude of interference oscillations compared to the case of zinc prevalence. This is attributable to the fact that the overabundance of tellurium in the volume of the grown film provokes the formation of defects that absorb a significant part of the radiation. Comparison of the dependences $\psi(\lambda)$ (Fig. 3) obtained from different regions of the grown ZnTe structures (Fig. 2) shows that the energy positions of the critical points IFx4xxE, $E_1 + \Delta_1$, and the absorption depend on the ratio of the molecular fluxes of zinc and tellurium, but not on the film thickness. Fig. 4, representing the dependence of the parameter ψ on the wavelength of incident radiation for ZnTe sample № 21, shows that the positions of the extrema E_1, $E_1 + \Delta_1$, within the error limit do not depend on the measurement area. Thus, these values can be used as an estimate of the degree

Table 1. Energy positions and wavelengths for critical points observed in ZnTe samples № 21 and № 22

Critical point	№ 21				№ 22			
	ε_2		ψ		ε_2		ψ	
	E, eV	λ, nm	E, eV	λ, nm	E, eV	λ, nm	E, eV	λ, nm
E_0	2.25	550	2.27	546	2.27	546	2.25	550
E_1	3.66	339	3.65	340	3.64	341	3.65	340
$E_1 + \Delta_1$	4.22	294	4.27	290	4.22	294	4.24	292

Table 2. Energy positions and wavelengths of critical points observed in ZnTe sample No. 21 across different film regions, as determined using $\psi(\lambda)$ and $\varepsilon_2(\lambda)$ spectra

Critical point	Thickness, nm	Wavelength, nm		Energy, eV	
		ε_2	ψ	ε_2	ψ
E_1	174 342 213	339 340	340 	3.66 3.65	3.65
$E_1+\Delta_1$	174 296 213	294 295	290 	4.22 4.2	4.27
E_0	174 553 213	550 556 551	546 2.24 545	2.25 2.23 2.25	2.27 2.27

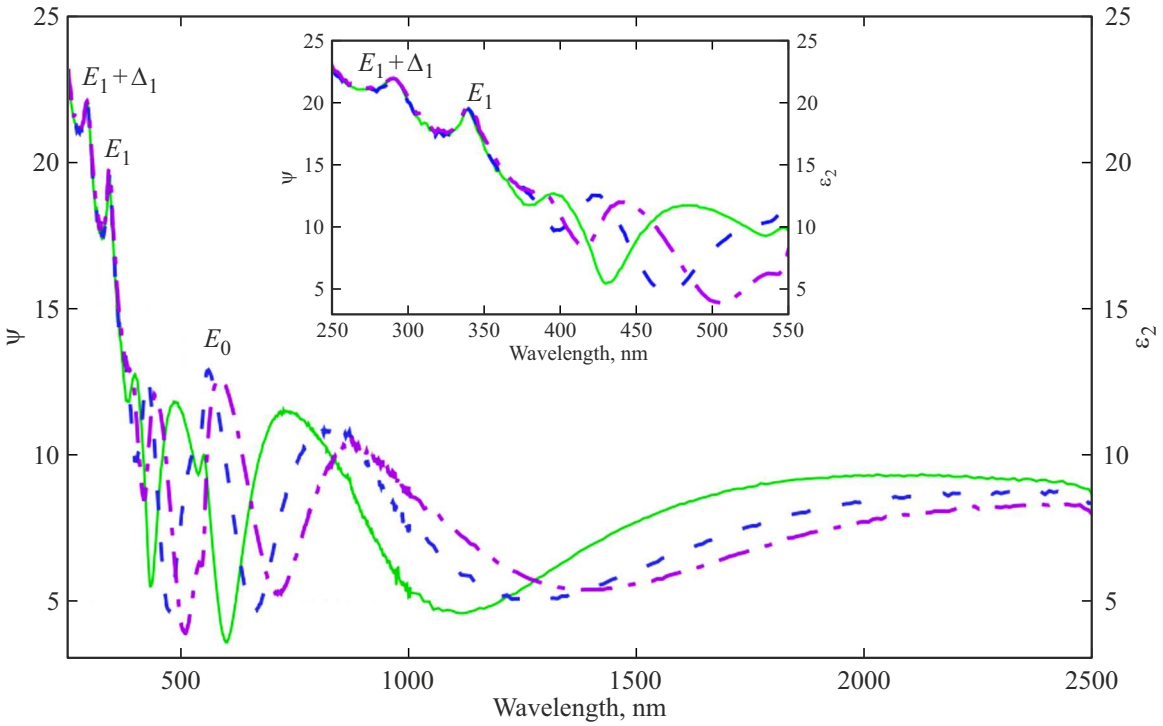

Figure 4. Dependence of the parameter ψ on the wavelength of the incident radiation for ZnTe sample № 21. The solid curve shows the first region of the film, the dashed curve shows the second region of the film, the dashed curve shows the third region of the film. Extremes corresponding to the critical points of the structures are marked.

of single crystallinity and composition stoichiometry in the ZnTe binary compound.

The difference in the ellipsometric spectra of the parameter ψ of ZnTe samples № 21 and № 22 is caused by the peculiarities of the epitaxial growth kinetics of the epitaxial growth of the group of solid solutions A_2B_6. An amorphous tellurium layer is initially formed on the GaAs substrate in the case of the ZnTe sample № 22 because of the filling of the broken gallium bonds with tellurium atoms [8,23]. Once on the surface of the growing film, ZnTe molecules begin to migrate across it in search of nodes with minimal potential energy and, having found them, form bonds with near-surface tellurium atoms. Due to the excessive content of Te_2 molecules in the crystal structure of the epitaxially growing layer, tellurium precipitates are formed, which can subsequently form cluster complexes. Their high concentration, in turn, reduces the crystal quality and optical characteristics of the ZnTe layer by absorbing the incident radiation energy. Therefore, to stabilize the ZnTe surface, it is necessary to maintain the composition stoichiometry of Zn:Te greater than or equal to two [9]. To test this hypothesis, the flux of the incident binary compound was increased in the case of the № 21 sample by including an additional zinc source in the growth process. It can be seen from Fig. 4 that a decrease of the absorption of incident radiation by the sample and, consequently, a decrease of the amplitude of the extremum on the ellipsometric spectrum are consequences of the stabilization of the surface by zinc. The grown ZnTe film became more transparent to visible and IR radiation.

Fig. 4 shows that despite the same character of energy location of critical points E_1, $E_1 + \Delta_1$ in the plane of one sample, there is a shift of ellipsometric pattern depending on the choice of measurement point (Fig. 2). The amplitude of interference oscillations decreases in the transparency region ($E < E_g$) with the increase of the film thickness.

The thickness gradient of the sample № 21 was acquired using the ellipsometric method (Table 2), and confirmed by scanning electron microscopy (SEM), the results of which are shown in Fig. 5. The ZnTe film has a non-uniform thickness as can be seen from Fig. 5, which agrees well with ellipsometric data.

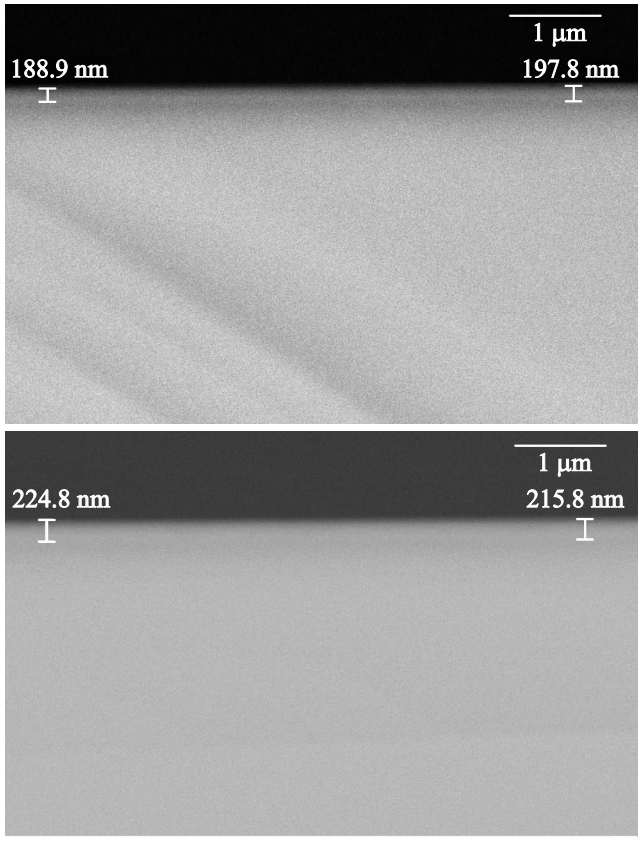

Figure 5. Results of determination of thickness of ZnTe sample № 21 using a scanning electron microscope.

Conclusions

The ellipsometric spectra of the parameter IFx3xxE of samples with different stoichiometry of Zn:Te composition were analyzed in this study. It is shown that the Van-Hove features E_1, $E_1 + \Delta_1$ are sensitive to the stoichiometric composition of the film. The comparison of the spectra showed that the prevalence of one of the components in the Zn:Te ratio changes the amplitude of the extrema. The energy positions of the critical points do not change when the thickness of the films varies. Therefore, it is sufficient to synthesize a relatively thin film (~ 100 nm) to analyze the Zn:Te flux ratio. However, the excess Zn in the Zn:Te ratio creates defects in the ZnTe structure compared to the case of Te prevalence, despite stabilization of the surface. This affects the accuracy of determination of the width of the band gap. The prevalent tellurium in the ratio Zn:Te increases the roughness of the film surface, so the interference extrema in amplitude are smaller than at zinc excess. Also, the energy position of the extrema corresponding to the critical points in the opacity region ($E > E_g$) in the dependences $\psi(\lambda)$ and $\varepsilon_2(\lambda)$ coincide within 0.15 nm for E_1 and within 5 nm for $E_1 + \Delta_1$. Consequently, sample roughness has a greater effect on the long-wavelength shift of the Van-Hove feature $E_1 + \Delta_1$ than on the shift E_1. Thus, it is possible to perform a rapid analysis of composition stoichiometry and evaluate the crystalline quality of ZnTe films based on $\psi(\lambda)$ without using spectra ε.

Acknowledgments

The authors would like to express their gratitude to V.A. Malygin, the 2nd category engineer of the JSC NPO ORION, for SEM measurements.

Conflict of interest

The authors declare that they have no conflict of interest.

References

[1] F. Hou, Y. Zhang, Y. Zhou, M. Zhang, B. Lv. Sustainability, **14** (18), 11161 (2022). DOI: 10.3390/su141811161
[2] T. Kawanishi. Photonics, **8** (5), 160 (2021). DOI: 10.3390/photonics8050160
[3] D. Wang, M.L. Kuzma, X. Tan, T.C. He, C. Dong, Z. Liu. J. Adv. Drug Delivery Rev., **179**, 114036 (2021). DOI: 10.1016/j.addr.2021.114036
[4] S. Durganjali, S. Bethanabhotla, S. Kasina, S. Radhika. J. Physics: Conf. Ser., **1495**, 012018 (2020). DOI: 10.1088/1742-6596/1495/1/012018
[5] H.L. Liu, C.C. Chen, C.C. Yeh, C.H. Chen, M.Y. Yu, S. Keller, S.P. DenBaars. Chem. Phys. Lett., **345** (3-4), 245-251 (2021). DOI: 10.1016/S0009-2614(01)00858-2
[6] V.S. Varavin, S.A. Dvoretskii, N.N. Mikhailov, V.G. Remesnik, I.V. Sabinina, Yu.G. Sidorov, V.A. Shvets, M.V. Yakushev, A.V. Latyshev. Optoelectron. Instrument. Data Process., **56**, 456-469 (2020). DOI: 10.3103/S8756699020050143
[7] H. Singh, T. Singh, J. Sharma. ISSS J. Micro Smart Syst., **7**, 123-143 (2018). DOI: 10.1007/s41683-018-0026-2
[8] R.D. Feldman, R.F. Austin, A.H. Dayem, E.H. Westerwick. Appl. Phys. Lett., **49**, 797, 1986. DOI: 10.1063/1.97550
[9] R.D. Feldman, R.F. Austin, P.M. Bridenbaugh, A.M. Johnson, W.M. Simpson, B.A. Wilson, C.E. Bonner. J. Appl. Phys., **64**, 1191 (1988). DOI: 10.1063/1.341883
[10] T. Moss, G. Barrell, B. Ellis. *Semiconductor Optoelectronics* (Mir, M., 1976), p. 56.
[11] K.V. Shalimova. *Fizika poluprovodnikov* (Energoatomizdat, M., 1985), ed. 3, p. 302 (in Russian).
[12] V.A. Shvets, M.V. Yakushev. Opt. Spectrosc., **92** (5), 780-783 (2002). DOI: 10.1134/1.1481146
[13] F. Ahmed, A.E. Naciri, J.J. Grob, M. Stchakovsky, L. Johann. Nanotechnology, **20**, 305702 (2009). DOI: 10.1088/0957-4484/20/30/305702
[14] E.D. Palik. *Handbook of optical constants of solids* (Academic Press, USA, 1998), V. 1−3, P. 798.
[15] V. Gupta, A. Mansingh. J. Appl. Phys., **80**, 1063-1073 (1996). DOI: 10.1063/1.362842
[16] V.A. Shvets, D.V. Marin, V.G. Remesnik, I.A. Azarov, M.V. Yakushev, S.V. Rykhlitsky. Opt. i spektr., **128** (12), 1815-1820 (2020) (in Russian). DOI: 10.21883/OS.2020.12.50315.349-20
[17] D.V. Marin, V.A. Shvets, I.A. Azarov, M.V. Yakushev, S.V. Rykhlitskii. Infrared Phys. Technol., **116**, 103793 (2021). DOI: 10.1016/j.infrared.2021.103793
[18] V.A. Shvets, D.V. Marin, M.V. Yakushev, S.V. Rykhlitsky. FTP, **57** (6), 469-475 (2023) (in Russian). DOI: 10.61011/FTP.2023.06.56476.5278
[19] V.A. Shvets, I.A. Azarov, D.V. Marin, M.V. Yakushev, S.V. Rykhlitsky. FTP, **53** (1), 137-142 (2019) (in Russian). DOI: 10.21883/FTP.2019.01.47001.8947
[20] F.T.J. Smith. J. Phys. Chem. Sol., **32** (9), 2201-2209 (1971). DOI: 10.1016/S0022-3697(71)80398-0
[21] I. Horichok, T. Parashchuk, M. Pylyponiuk, O. Soroka, M. Voloshynovych. J. Crystal Growth, **486**, 10-18 (2018). DOI: 10.1016/j.jcrysgro.2017.12.039
[22] K. Sato, S. Adachi. J. Appl. Phys., **73**, 926-931 (1993). DOI: 10.1063/1.353305
[23] G. Cohensolar, F. Bailly, M. Barbe. Appl. Phys. Lett., **49**, 1519 (1986). DOI: 10.1063/1.97320

Translated by A.Akhtyamov